Design of a Bidirectional Rotational Motion actuator by SMA with geometrico-static requirements

Kejun Hu[a], Morvan Ouisse[a], and Kanty Rabenorosoa[a]

[a]FEMTO-ST Institute, Univ. Bourgogne Franche-Comté, CNRS, 26 chemin de l'épitaphe, Besançon, France

ABSTRACT

Shape memory alloys (SMAs) are a group of metallic alloys capable of sustaining large inelastic strains that can be recovered when subjected to a specific process between two distinct phases. Advantages of SMAs - reasonable strain, high energy density, mechanical simplicity, and long work-life render them ideal for actuator applications. Especially, Self-folding origami requires high angular motion ranges and low-profile actuators within limited space. Current applications demonstrate the capacity of millimeter-sized torsional SMAs (T-SMAs) for bi-directional rotational motion, but no comprehensive design method for such actuators can be found in the existing literature. To broaden applications of actuator designs, we introduce an inverse design model according to a geometrico-static demand. We couple the geometrical and mechanical properties of torsional SMAs considering assembly and working conditions to construct the design model. We also illustrate a comprehensive mechanical performance characterization for millimeter-sized torsional SMAs and BRM actuators.

Keywords: shape memory alloy, origami robot, self-folding, modeling, bi-directional rotational motion

1. INTRODUCTION

SMAs made of nickel and titanium (Nitinol) have attracted wide interest in both research[1,2] and industry[3,4] thanks to their outstanding properties such as high energy density,[5] reasonable operational strain relying on shape memory effect, mechanical simplicity, and long work life. Integrated into smart composites, these properties can be used to actuate folding.[6] Origami provides a means of transforming thin tessellated panels into 3D form with many unique and desirable structural properties such as auxetics, tunable stiffness, and multistability.[7,8] Moreover, robots inspired by folding mechanical structures known as 'Origami robots' gained much attention recently. As for the robotics field, the introduction of origami engineering enables 'semi-rigid' properties.[9] By means of actuation of origami robots using SMA, variety of actuators were introduced in last decades: uni-directional rotational motion[10,11] and bi-directional rotational motion (BRM).[12–14] Previous works[15] provided a review of SMA-based actuation of state of the art in SMA-based actuators for BRM. Additionally, the torsional-SMA-based actuators (T-SMAs) showed an exciting potential for the BRM actuation of meso-scale origami robotics. However, due to the SMA's highly nonlinear hysteretic and temperature-depended behavior, the BRM actuators designing and characterizations are proven to be challenging. Concerning the SMA-based design, the stress-strain/force-displacement diagram on which the austenite curve of the active element and the hosting structure is frequently mentioned as a valuable and effective tool.[16] Previous works have shown that this method is acceptable not only for a single SMA device but also for antagonist designing.[15] However, the method is based on a fixed dimension of the SMA element. Thus studies usually focus on designing the bias element [*]. In fact, the ability due to shape memory effect (SME) of an SMA according to a certain temperature is well described by its 'M→A curve' so-call 'Austenite curve', which can be identified and modeled using the method described in.[15] Regarding the experimental characterization of torsional SMAs, two characterization approaches are frequently mentioned in the literature: the isobaric test and isotherm tests. The former is performed by

---

Further author information:
K.Hu: E-mail: kejun.hu@femto-st.fr
M.Ouisse: E-mail: morvan.ouisse@femto-st.fr
K.Rabenorosoa: E-mail: rkanty@femto-st.fr

[*] for example, a passive biased spring with different stiffness[17]

holding constant stress and sweeping temperature up and down while measuring the strain response, relying on the shape memory effect of SMAs. The latter is performed by holding constant temperature and sweeping the strain up and down while measuring the axial load response, relying on the pseudo-elastic (pure Austenite phase) and inelastic behavior (partial or pure martensite phase).[18] However, these experimental approaches require precise multi-physical controlling for thermal and mechanical conditions. Consequently, very limited experimental results of millimeter-sized actuator using T-SMA can be found in the literature. This work aims to develop a design model of a BRM actuator using SMA constitutive laws according to a geometrico-static demand. The main contributions of this research are: 1) development of a direct designing model using four design parameters; 2) experimental characterizations of the millimeter-scale T-SMAs actuator; 3) an inverse design methodology for a BRM actuator using T-SMAs for origami robots.

2. METHODS

2.1 Constitutive model

The three-dimensional phenomenological Lagoudas constitutive model[19] is utilized in this work. This constitutive model starts with the definition of the Gibbs energy G. The energy function G is described by the set of independent state variables $(\sigma, T, \xi, \varepsilon^t)$, which describe the stress, the temperature, the martensitic volume faction, and the transformation strain. The explicit form of the Gibbs free energy is given by,

$$\begin{aligned} G\left(\sigma, T, \xi, \varepsilon^t\right) \quad = \quad & -\frac{1}{2\rho}\sigma : \mathcal{S} : \sigma - \frac{1}{\rho}\sigma : \left[\alpha\left(T - T_0\right) + \varepsilon^t\right] + c\left[\left(T - T_0\right) - T\ln\left(\frac{T}{T_0}\right)\right] \\ & - s_0 T + u_0 + \frac{1}{\rho} f(\xi) \end{aligned} \tag{1}$$

where ρ is the mass density, $\mathcal{S}$ the effective compliance tensor, α the effective thermal expansion coefficient, c the effective specific heat, s_0 the effective specific entropy, and u_0 the effective internal energy reference state. The effective compliance tensor $\mathcal{S}$ is determined using a parallel Voigt model of properties according to two pure phases and the martensitic volume fraction ξ via the following expression:

$$\mathcal{S}(\xi) = \xi \mathcal{S}_M + (1 - \xi)\mathcal{S}_A = \mathcal{S}_A + \xi \Delta \mathcal{S} \tag{2}$$

where the subscripts A and M denote the austenitic and martensitic phases, respectively. The symbol $\Delta(\cdot)$ indicates the difference between the pure martensitic and austenitic phases. Also, other material parameters α; c; s_0; u_0 are averaged this way. To describe the interaction kinematic between the martensitic and austenitic phases, a hardening function $f(\xi)$ is introduced. As indicated in,[19] the hardening function can be written into different form according to the same state variable set: 1) exponential form,[20] 2) cosine form,[21] 3) polynomial form.[22] For example, a hardening function in cosine form is given by,

$$f(\xi) = \begin{cases} \int_0^{\xi} -\frac{\rho \Delta s_0}{a_c^M}\left[\pi - \cos^{-1}(2\xi - 1)\right] d\xi + \left(\mu_1^c + \mu_2^c\right)\xi; & \dot{\xi} > 0 \\ \int_0^{\xi} -\frac{\rho \Delta s_0}{a_c^A}\left[\pi - \cos^{-1}(2\xi - 1)\right] d\xi + \left(\mu_1^c - \mu_2^c\right)\xi; & \dot{\xi} < 0 \end{cases} \tag{3}$$

where $a_c^M, a_c^A, \mu_1^c, \mu_2^c$ are transformation strain hardening model parameters. The inequality of martensitic volume fraction rate $\dot{\xi}$ denote the phase transformation direction. For example, $\dot{\xi} > 0$ presents a forward phase transformation $(A \rightarrow M)$, and vice versa. The constitutive relation is determined using Gibbs free energy as

$$\varepsilon = -\rho \frac{\partial G}{\partial \sigma} = \mathcal{S} : \sigma + \alpha\left(T - T_0\right) + \varepsilon^t, \tag{4}$$

based on the assumption that any change in the material's current state relies on a change of the martensite volume fraction. The evolution equation of transformation strain and the martensitic volume fraction is obtained as,

$$\dot{\epsilon} = \Lambda \dot{\xi} \tag{5}$$

where Λ is the normalized transformation tensor that changes principal directions depending on the direction of the martensitic transformation. The expression is given as

$$\Lambda = \begin{cases} \frac{3}{2}H\frac{\sigma'}{\bar{\sigma}'}; & \dot{\xi} > 0 \\ H\frac{\varepsilon^{t-r}}{\bar{\varepsilon}^{t-r}}; & \dot{\xi} < 0 \end{cases} \tag{6}$$

where $H, \sigma', \bar{\sigma}', \varepsilon^{tr}, \bar{\varepsilon}^{tr}$ are the maximum transformation strain, the deviatoric stress tensor, the von Mises equivalent stress, the transformation strain tensor at at the reversal point and the effective transformation strain, respectively.

2.2 Numerical model

An FEA-based geometrico-quasi-static model is constructed using an SMA torsional rod in the commercial software COMSOL. The aforementioned constitutive laws using the cosine form hardening function is implemented. As the diameter of the rod is small with respect to its length, only a representative (unit) segment of an SMA rod is developed.[19] Model features including geometry parameters (diameter and length) and material properties are chosen to compare those reported in experimental studies performed by,[23] thus providing an experimental baseline for this study. The rods were characterized in that work had three different diameters measuring around 0.5 mm and a constant length of 10.16 mm. The pseudo-elastic behavior of each sample at room temperature was characterized. It is worth mentioning that, due to the non-uniform shear stress distribution, the angle versus torque relationship relies on the material properties and the geometry. Compared to an SMA with a tensile test, the return of elastic behavior after a complete phase transformation is less obvious. The comparison between experimental results and simulation results is shown in Figure 1 B). The FE model can capture the influence of sample dimension on the angle versus torque pseudo-elastic relationship. Moreover, the criteria points such as the start and finish points according to both $M \rightarrow A$, and $A \rightarrow M$ transformation are accurately captured. Therefore, this model is consequently utilized for the designing of the BRM actuation using antagonist arrangement in the following.

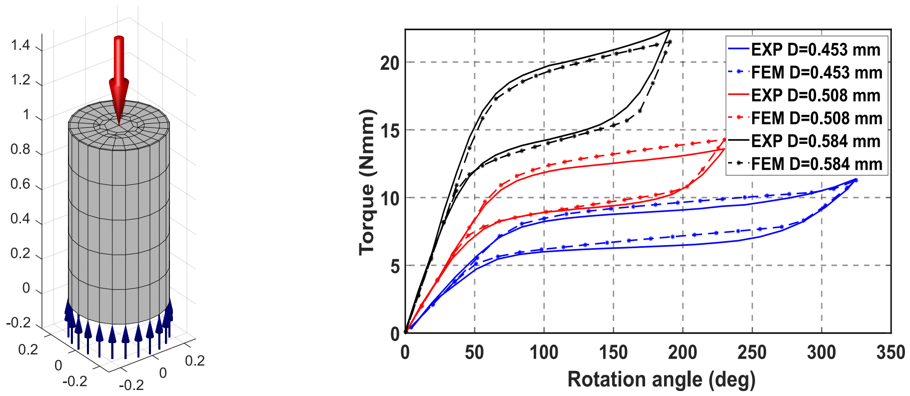

(a) (b)

Figure 1: Simulation results of a pseudo-elastic SMA-based torsional element: a) boundary conditions for the rod, red arrows represents the applied torque, blue arrows represent the fixed constraint boundary condition; b) comparison between experimental results and simulation results, the experimental data is from.[23]

2.3 Forward model of BRM actuator for designing

A system consisting of two antagonists, so-called 'active-biased' SMA elements, is implemented in this work. Regarding the bi-directional rotational motion, an SMA-based actuator has to meet two requirements: the output torque and the motion range. In this case, four design parameters are taken into account: 1) The dimension of elementary SMA: radius r and length L of an SMA element. 2) The position angle of actuator θ: regarding the antagonist design, the maximal folding angle that the actuator can realize depends on the prestrain/pre-twisting

SMA elements. This prestrain presents the strain that the SMA torsional rod undergoes when the folding hinge to be actuated is in its original position and the elementary SMA in the passive state. For a prescribed prestrain of both SMA elements, the motion range of the actuator is determined by the intersection of the austenite characteristics of the activated SMA element and the total payload torque. 3) The maximum activated temperature T: conventional SMA designing usually uses a straight form curve with Young's modulus corresponding to the pure austenitic phase.[16,24] However, the SMAs' phase transition temperature highly depends on the applied stress. Thus a biased SMA requires a higher temperature to achieve the transition. The overheating is indicated in the literature as a risk of degradation of SMA components and structure material.[25] In this work, the structure to be activated utilizes polyester material, exhibiting relatively low thermal stability regarding the functional origami structure. The maximum temperature should have be taken into account. The actuation performance based on SME of an SMA at a specific temperature is accurately described by its ‘Austenite curve, which can be modeled using the method described in 2.1. Here, a torque-angle-radius [†] iso-temperature surface is introduced in order to address the influence of the parameters as mentioned above on actuator performance. A parametric analysis is performed via the unit length SMA model based on variable radius and temperature. Twelve different radii between 0.25mm to 0.5mm and three temperatures above the finish transition temperature A_f are considered. According to the average martensite volume fraction rate $\dot{\bar{\xi}}$, thirty-six M→A curves are obtained. Those curves are then interpolated non-linearly using mathematical tools [‡]. It is worthing to remind that the implemented constitutive model does not consider the stress-induced reorientation (detwinning) of the martensite phase at low temperatures. Consequently, a virtual passive surface with modified material properties is realized to provide a similar mechanical response (see figure 5) to characterization results. We use the intersection curve between the active iso-temperature surfaces and virtual passive surfaces to predict actuator performance relying on actuator dimension and positioning angle at a specific temperature. Assuming that the antagonistic SMA are identical, only one active surface in the clockwise direction and a passive surface in the anti-clockwise direction is sufficient. The working flow is given in the following: 1) The active curves are placed at the origin point, and the passive curves are placed with a particular position angle. The two surfaces are then implemented using a grid density of 1000×1000 points. 2) The primary zone around the intersection curve is then determined using the mesh of the previous step. 3) The two localized surfaces are interpolated using mathematical tools in the primary zone. A local nonlinear solver is then used to detect the intersection point analytically according to every radius increment. Figure 3a shows an example of the intersection curve between an iso-surface at a temperature of $T = A_f + 70°C$ with a position angle of 14 degrees/mm. The solid white line presents the intersection curve

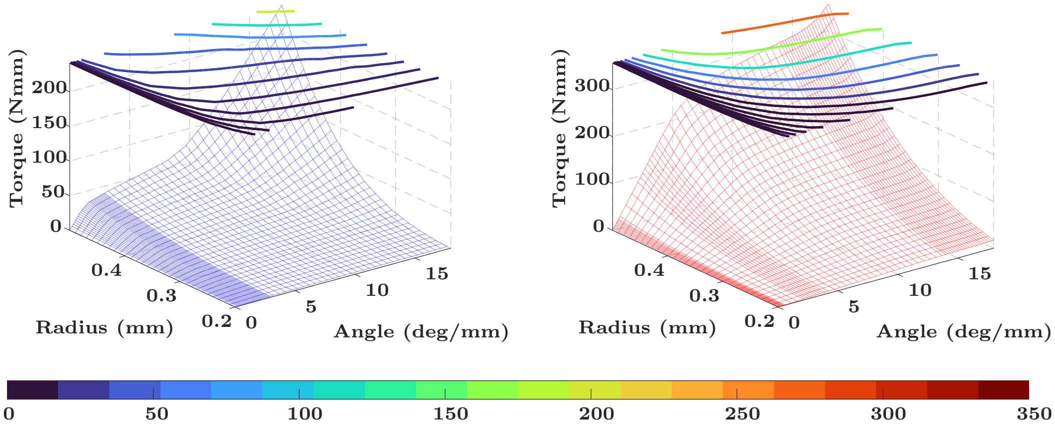

Figure 2: Examples for iso-temperature surfaces using identified parameters. The image on the left presents the virtual passive surface at room temperature, and the image on the right shows the unit length actuator performance at $A_f + 70°C$.

[†] The angle here is a unit length rotation angle

[‡] in this case, the data are fitted using 'griddata' code via Matlab

between two surfaces, and the solid black line illustrates the maximum output torque during the whole stroke. It is trivial to observe that the radius and the motion range at this position angle exhibit a nonlinear relationship.

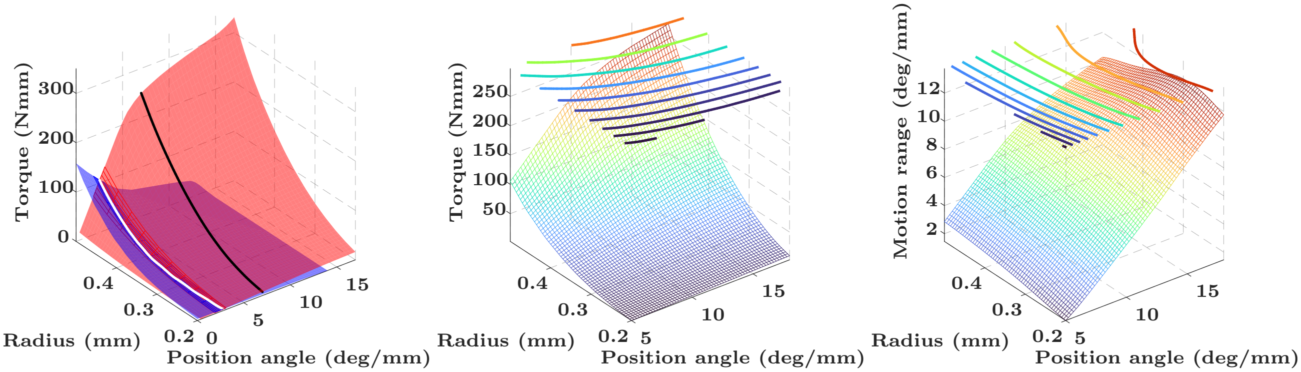

(a) (b) (c)

Figure 3: An example of forward model for designing: a) an example for intersection curve assuming identical antagonistic T-SMAs activated at $A_f + 70°$ pre-twisted at a unit rotation angle of 14 degrees; b) an example of maximum output torque surface for different radius and different position angle; and c) an example of motion range surface for different radius and different position angle.

2.4 Experimental characterization of T-SMAs

Actuator modelling requires a precise understanding of mechanical performance. The results of SMAs depend on test thermomechanical history due to their high hysteresis. In order to test the static response of the material, torque–angle measurements were performed with the electrothermal controller that maintained at a constant temperature. The objective of the test is to identify the material parameter using the FEA mentioned earlier. As shown in figure 4, the experimental setup consists of a torque sensor for (FUTEK TDD400) measuring the applied torque on T-SMA, a motion controller (brushed servo-motor: Dynamixel XM430) with a linear rail for providing a pure torsional load. For the thermo-mechanical condition control, a close-loop with PI-controller is used with

the torque sensor's feedback. Two samples (Dynalloy flexinol) with a dimension of 0.5mm diameter and

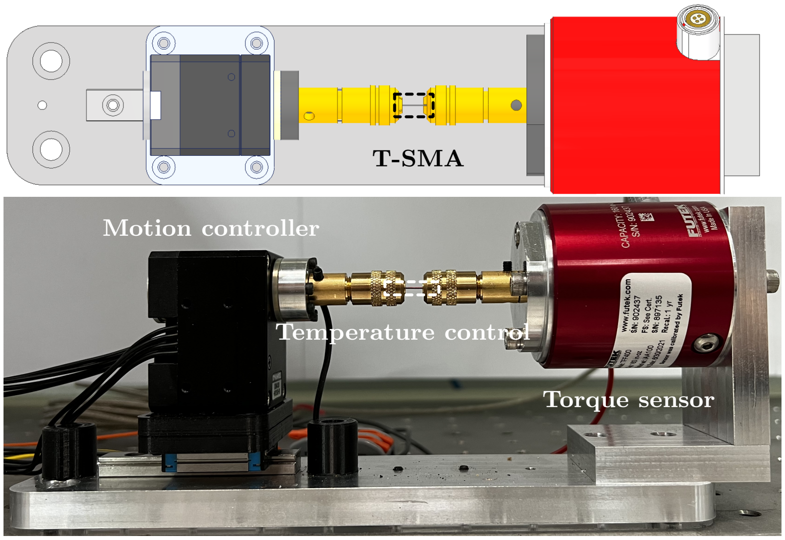

Figure 4: Experimental setup for charaterization of T-SMA actuator

5.4mm length are tested in this case. The specimen is held using a drill chuck with split collet grips. Therefore the slippage during the isotherm test is eliminated. The samples have a coil 'shape' as initial memory. Thus all the samples are annealed in a mold at 430 degrees Celsius for 30 mins, then quenched in water to memorize a straight and untwisted shape. Concerning the isotherm test, seven temperatures between room temperature and higher temperatures are tested with five cycles at a constant rotation rate of 3 degrees/s. Both torque captured by the sensor and rotation angle given by the servomotor are then recorded to obtain the curve torque versus angle of the wires for different temperatures (see figure 5).

3. RESULTS

3.1 Characterization results

Figure 5 shows the experimental characteristics of SME-based T-SMA at different temperatures show the inelastic and pseudoelastic characteristics. The test results at room temperature are shown using the black dash line. It is trivial that the material yields an elastic stiffness until it achieves a 4Nmm torque, then detwinning starts and finishes at a torque of 10Nmm. A considerable amount of twisting angle is observed after an elastic release (80 degrees). Subsequently, load provides an elastic response with similar stiffness; thus, a typical elastoplastic behavior with small hysteresis is observed at room temperature. On the other hand, complete PE recovery is observed experimentally at a temperature higher than $35°C$. The variations induced thermal stimulus on the start and finish criteria point of both M→A and A→M transformation are observed. Regarding the 26Nmm maximum torque, the increasing temperature reduces rotation stroke from 156 degrees to 81 degrees. Similar observation at a larger scale was reported in.[26] One important difference is that in the SME T-SMAs comparing the PE T-SMAs (see figure 1 b)), the PE behaviors showed a smaller hysteresis compared to existing data of PE T-SMAs in the literature.[23, 27] Additionally, a significant deviation of the start criteria of M→A transformation (beginning point of PE recovery) induced by a small difference of temperature is observed (see curves according to 35, 40 and $42°C$). The identified model parameters are shown in table 1.

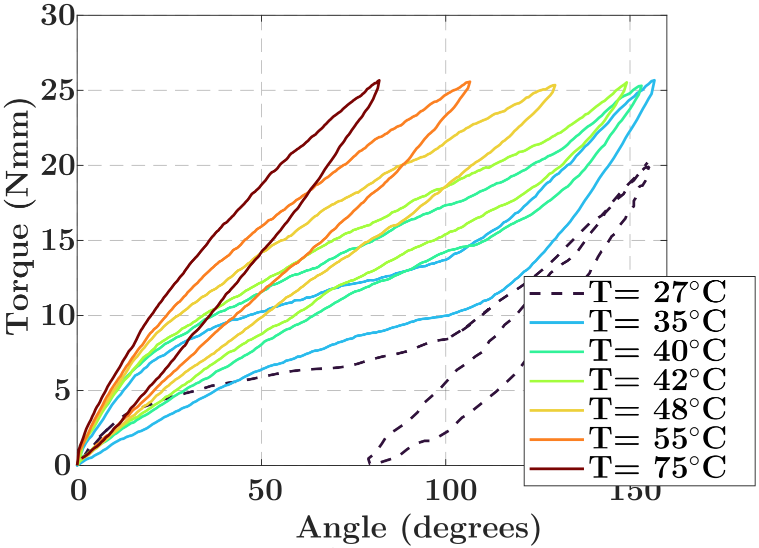

Figure 5: The isotherm test results: Torsion test of two 0.5mm diameter and 5.4mm length wires undergoing five cycles at seven temperatures. Ramp form loading/unloading torque with a maximum value of 26Nmm is cyclically applied at a rotation rate of 3 degree/s.

3.2 Parametric analysis results

Figure 6 and figure 7 show the parametric analysis results via the direct model using the identified material properties. The motion range and the maximum output torque are computed versus the actuator dimension

Table 1: Identified Model parameters of tested T-SMA samples: M: PE represents pseudo-elastic behaviors at temperatures above A_f, and VP represents the virtual passive response at room temperature.

Model parameter				
Symbols	Description	Values		Units
		PE	VP	
E_M	Elastic Modulus of Martensite	41	38	GPa
E_A	Elastic Modulus of Austenite	65	38	GPa
M_f	Martensite Finish Transformation Temperature	0	16	$°C$
M_s	Martensite Start Transformation Temperature	25	26	$°C$
A_s	Austenite Start Transformation Temperature	8	-	$°C$
A_f	Austenite Finish Transformation Temperature	33	-	$°C$
C_M	Stress Influence Coefficient of Martensite	31	25.5	MPa/$°C$
C_A	Stress Influence Coefficient of austenite	30.3	25.5	MPa/$°C$
ϵ_L	maximum transformation strain	0.0299	0.0299	

and the position angle according to three activation temperature. As shown in the figure 6, an increase of elements' radius and a decrease of position angle induce the increase of output torque. Additionally, an increase of output torque around 100% can be obtained by increasing the activation temperature from $A_f + 20°C$ to $A_f + 70°C$ thanks to the high stress influence coefficient of austenite. On the other hand, the relation between the motion range, the actuator radius, and the large position angles yields a highly nonlinear relationship. For a position angle less than 12 degrees/mm, the motion range is dominated by the position angle. However, for a BRM actuator with a position angle larger than 12 degrees/mm (equivalent to 180 degrees with a 15mm length actuator), local optimum of motion range is obtained with a radius equal to 0.3mm for all three cases. Regarding the technical demand for self-folding application, the folding stiffness belongs from 0.106Nmm/mm/rad to 2.1Nmm/mm/rad[28](for example the stiffness are [0.037,0.7330]Nmm/deg for 20mm length hinge). Even with a small radius, a BRM actuator is capable of providing a typical 'open-close' self-folding motion. However, origami structures that induce geometrical nonlinearity (aka 'non-rigid' origami), or material nonlinearity (for example, 'thick-panel-origamis' and 'polymer-based origamis') require higher actuation performance.[29] Consequently, an inverse design methodology is introduced to design a BRM actuator in a general manner.

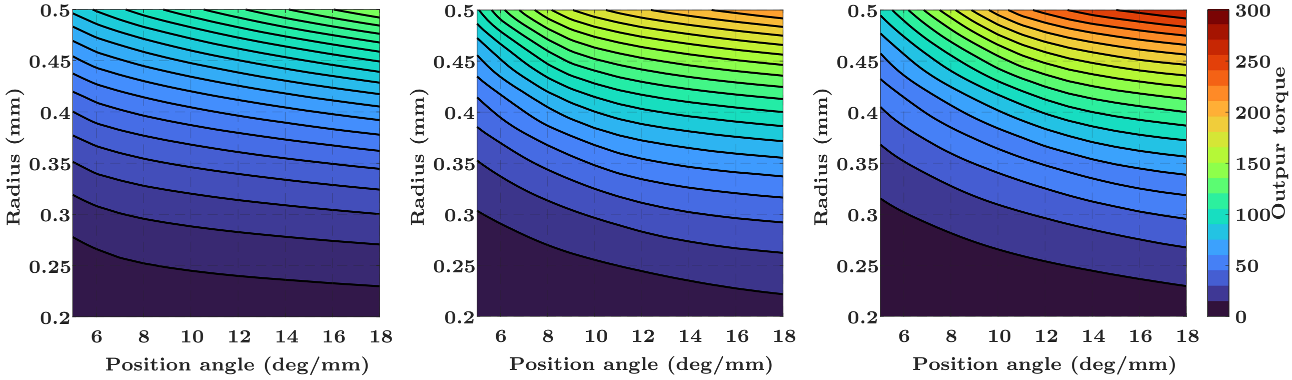

Figure 6: An example of BRM actuator output torque prediction using the inverse design model for temperature, the corresponding activation temperatures from left to right are: $A_f + 20°C$, $A_f + 50°C$ and $A_f + 70°C$

3.3 Inverse design model

A methodology for designing the BRM actuator is developed regarding the technical requirement according to origami robots. This method couples the aforementioned direct design model and loop-form mechanical feature

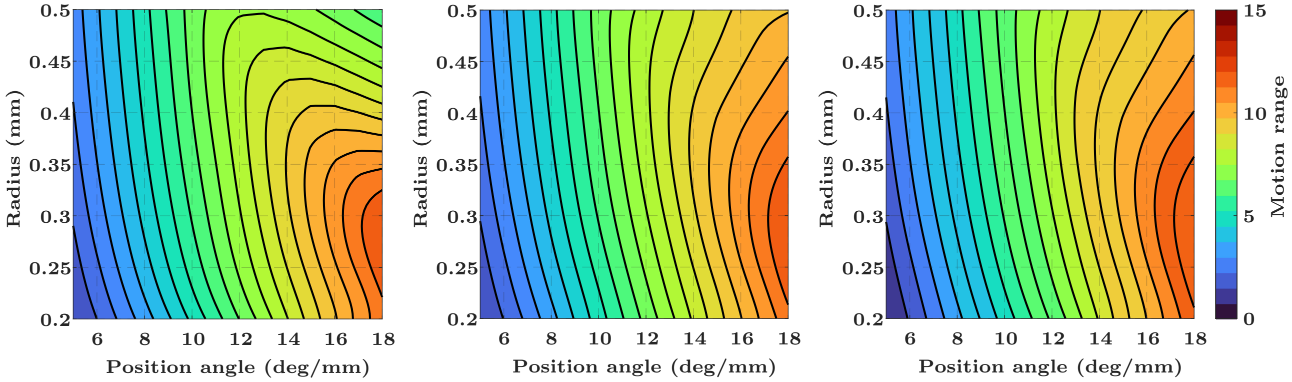

Figure 7: An example of BRM actuator motion range prediction using the inverse design model for temperature, the corresponding activation temperatures from left to right are: $A_f + 20°C$, $A_f + 50°C$ and $A_f + 70°C$

to identify the actuator dimensions for an origami structure that capable of 'shape-changing'. The proposed design methodology is shown in figure 8:

1. In the system requirement block, a structure's single or multiple shape morphing are defined first, locally or globally[11,30]). According to each shape morphing strategy, the necessary performance can be determined using experimental characterization of prototype or modelling.
2. In the choice of the material bloc, a proper SMA adapted to an application should be determined. This selection should be based on system constraints and requirements, which include the torque and stroke, surrounding and actuator temperatures, fatigue, energy consumption, and the working environment conditions.
3. After the selection of SMA material, the properties mentioned in 2.1 are mandatory for the performance prediction.
4. In the thermochemical modelling block, the torque-angle-radius iso-temperature surface presented in 2.3 is etablished to identify the dimension of SMA element and the position angle that answers the system requirement.
5. A characterization on the whole system to validate the designing of the actuator, the design process will be finished if the technical requirements are attained. If it is not the case, the design loop will re-begin at actuator dimensions for another iteration with modification.

These are the indications for the design process for the dimensioning of a antagonistic BRM actuator using T-SMA; all the considerations are valid for both commercial torsional wires or home made samples.

4. CONCLUSION

A design model has been established for the design of a BRM actuator activated by antagonist T-SMAs. The model is constructed via a unit-length T-SMA FEA model using Lagoudas three-dimension constitutive law. Four design parameters are considered to meet the actuator requirements (motion range and output torque). Two design approaches are introduced according to the different design problems. Regarding the direct design method, a parametric analysis is performed to understand the influence of each parameter on actuator performance. The results showed that a tuning of elements' radius and position angle induces a performance modification. Regarding the inverse design model, a loop-form mechanical design feature is introduced for prototype fabrication and characterization of the BRM actuator for specific application requirements. To characterize the material parameters of T-SMAs, a benchmark for milimeter-sized SME-based T-SMAs is carried out. The model parameters according to T-SMA's inelastic bahavior and PE behavior are provided. Additional work is

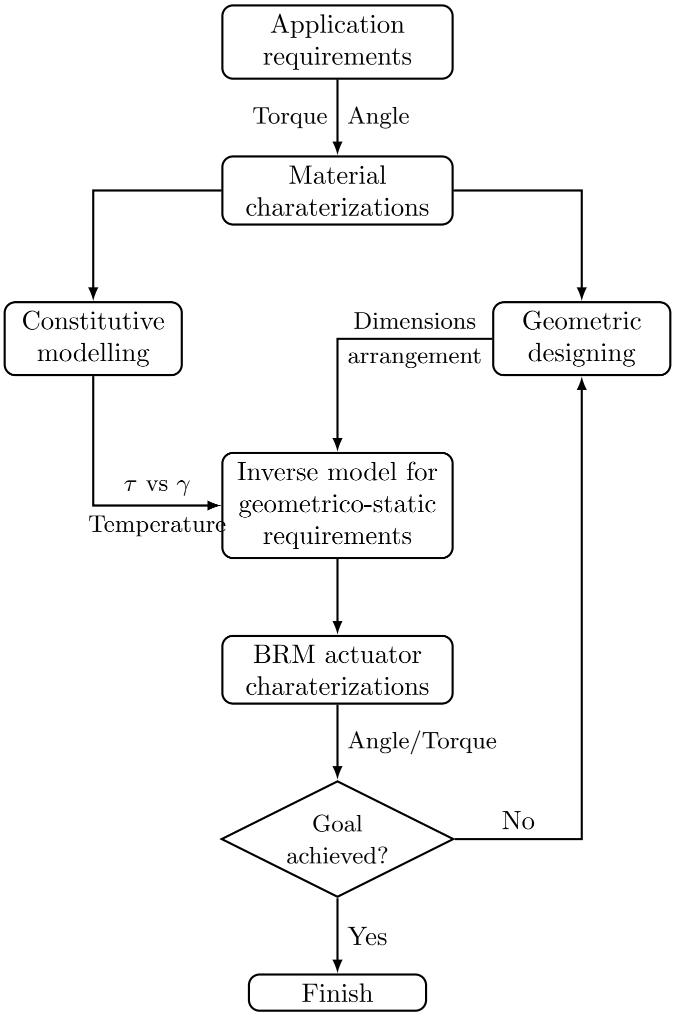

Figure 8: A loop form inverse design method of SMA-based BRM actuator

required to design and integrate the actuators for origami robots that are based on waterbomb and kresling patterns.

5. ACKNOWLEDGMENTS

The authors would like to acknowledge the financial support provided by the French National Agency for Research (OrigaBot ANR-18-CE33-0008), and EUR EIPHI (Contract No. ANR-17-EURE-0002).

REFERENCES

[1] Lester, B. T., Baxevanis, T., Chemisky, Y., and Lagoudas, D. C., "Review and perspectives: shape memory alloy composite systems," *Acta Mechanica* **226**(12), 3907–3960 (2015).

[2] Rodrigue, H., Wang, W., Han, M.-W., Kim, T. J., and Ahn, S.-H., "An overview of shape memory alloy-coupled actuators and robots," *Soft Robotics* **4**(1), 3–15 (2017).

[3] Benafan, O., Moholt, M., Bass, M., Mabe, J., Nicholson, D., and Calkins, F., "Recent advancements in rotary shape memory alloy actuators for aeronautics," *Shape Memory and Superelasticity* **5**(4), 415–428 (2019).

[4] Stroud, H. and Hartl, D., "Shape memory alloy torsional actuators: a review of applications, experimental investigations, modeling, and design," *Smart Materials and Structures* **29**, 113001 (11 2020).

[5] Lee, H.-T., Kim, M.-S., Lee, G.-Y., Kim, C.-S., and Ahn, S.-H., "Shape memory alloy (sma)-based microscale actuators with 60% deformation rate and 1.6 khz actuation speed," *Small* **14**(23), 1801023 (2018).

[6] Rus, D. and Tolley, M., "Design, fabrication and control of origami robots," *Nature Reviews Materials* **3**, 101–112 (05 2018).

[7] Li, S., Fang, H., Sadeghi, S., Bhovad, P., and Wang, K.-W., "Architected origami materials: How folding creates sophisticated mechanical properties," *Advanced Materials* **31**(5), 1805282 (2019).

[8] [*An Origami-Based Tunable Helmholtz Resonator for Noise Control: Introduction of the Concept and Preliminary Results*], *Smart Materials, Adaptive Structures and Intelligent Systems* **Volume 1: Development and Characterization of Multifunctional Materials; Mechanics and Behavior of Active Materials; Bioinspired Smart Materials and Systems; Energy Harvesting; Emerging Technologies** (09 2017). V001T08A002.

[9] Benouhiba, A., Rougeot, P., Andreff, N., Rabenorosoa, K., and Ouisse, M., "Origami-based auxetic tunable helmholtz resonator for noise control," *Smart Materials and Structures* (jan 2021).

[10] Hawkes, E., An, B., Benbernou, N. M., Tanaka, H., Kim, S., Demaine, E. D., Rus, D., and Wood, R. J., "Programmable matter by folding," *Proceedings of the National Academy of Sciences* **107**(28), 12441–12445 (2010).

[11] Nayakanti, N., Tawfick, S. H., and Hart, A. J., "Twist-coupled kirigami cells and mechanisms," *Extreme Mechanics Letters* **21**, 17–24 (2018).

[12] Zhakypov, Z., Mori, K., Hosoda, K., and Paik, J., "Designing minimal and scalable insect-inspired multi-locomotion millirobots," **571**(7765), 381–386.

[13] Firouzeh, A. and Paik, J., "Robogami: A fully integrated low-profile robotic origami," *Journal of Mechanisms and Robotics* **7**(2) (2015).

[14] Kim, S.-R., Lee, D.-Y., Ahn, S.-J., Koh, J.-S., and Cho, K.-J., "Morphing origami block for lightweight reconfigurable system," *IEEE Transactions on Robotics* **37**(2), 494–505 (2021).

[15] Hu, K., Rabenorosoa, K., and Ouisse, M., "A review of sma-based actuators for bidirectional rotational motion: Application to origami robots," *Frontiers in Robotics and AI* **8**, 202 (2021).

[16] Ameduri, S., "Chapter 9 - design of sma-based structural actuators," in [*Shape Memory Alloy Engineering*], Lecce, L. and Concilio, A., eds., 245–274, Butterworth-Heinemann, Boston (2015).

[17] Liu, X., Liu, H., and Tan, J., "Mesoscale shape memory alloy actuator for visual clarity of surgical cameras in minimally invasive robotic surgery," *IEEE Transactions on Medical Robotics and Bionics* **1**(3), 135–144 (2019).

[18] Churchill, C., Shaw, J., and Iadicola, M., "Tips and tricks for characterizing shape memory alloy wire: Part 2—fundamental isothermal responses," *Experimental Techniques* **33**(1), 51–62 (2009).

[19] Lagoudas, D., [*Shape Memory Alloys: Modeling and Engineering Applications*], Springer ebook collection / Chemistry and Materials Science 2005-2008, Springer US (2008).

[20] Tanaka, K., "A thermomechanical sketch of shape memory effect: one-dimensional tensile behavior," *RES MECHANICA* **2**(3), 59–72 (1986).

[21] Liang, C. and Rogers, C. A., "One-dimensional thermomechanical constitutive relations for shape memory materials," *Journal of Intelligent Material Systems and Structures* **1**(2), 207–234 (1990).

[22] Lagoudas, D., Bo, Z., Boyd, J., and Qidwai, M., "Thermomechanical modeling of shape memory alloys and composites," in [*Structronic Systems: Smart Structures, Devices and Systems: Part I: Materials and Structures*], 197–246, World Scientific (1998).

[23] Chapman, C., Eshghinejad, A., and Elahinia, M., "Torsional behavior of niti wires and tubes: Modeling and experimentation," *Journal of Intelligent Material Systems and Structures* **22**(11), 1239–1248 (2011).

[24] Koh, J.-s., Kim, S.-r., and Cho, K.-j., "Self-folding origami using torsion shape memory alloy wire actuators," in [*International Design Engineering Technical Conferences and Computers and Information in Engineering Conference*], **46377**, V05BT08A043 (2014).

[25] Mohd Jani, J., Leary, M., Subic, A., and Gibson, M. A., "A review of shape memory alloy research, applications and opportunities," *Materials & Design (1980-2015)* **56**, 1078–1113 (2014).

[26] Prahlad, H. and Chopra, I., "Modeling and experimental characterization of sma torsional actuators," *Journal of Intelligent Material Systems and Structures* **18**(1), 29–38 (2007).

[27] Rao, A., Ruimi, A., and Srinivasa, A. R., "Internal loops in superelastic shape memory alloy wires under torsion–experiments and simulations/predictions," *International Journal of Solids and Structures* **51**(25-26), 4554–4571 (2014).

[28] Filipov, E., Liu, K., Tachi, T., Schenk, M., and Paulino, G., "Bar and hinge models for scalable analysis of origami," *International Journal of Solids and Structures* **124**, 26–45 (2017).

[29] Meloni, M., Cai, J., Zhang, Q., Sang-Hoon Lee, D., Li, M., Ma, R., Parashkevov, T. E., and Feng, J., "Engineering origami: A comprehensive review of recent applications, design methods, and tools," *Advanced Science* **8**(13), 2000636 (2021).

[30] Jianguo, C., Xiaowei, D., Yuting, Z., Jian, F., and Ya, Z., "Folding behavior of a foldable prismatic mast with kresling origami pattern," *Journal of Mechanisms and Robotics* **8**(3) (2016).